JACS
JOURNAL OF THE AMERICAN CHEMICAL SOCIETY

Article

pubs.acs.org/JACS

Intradimer/Intermolecular Interactions Suggest Autoinhibition Mechanism in Endophilin A1

Zhiming Chen, Ken Chang, Benjamin R. Capraro, Chen Zhu, Chih-Jung Hsu, and Tobias Baumgart*

Department of Chemistry, University of Pennsylvania, 231 South 34th Street, Philadelphia, Pennsylvania 19104, United States

Supporting Information

ABSTRACT: Endophilin A1 is a homodimeric membrane-binding endocytic accessory protein with a high dimerization affinity. Its function has been hypothesized to involve autoinhibition. However, the autoinhibition mechanism, as well as the physicochemical basis for the high dimerization affinity of endophilin in solution, have remained unclear. In this contribution, we use a Förster resonance energy transfer (FRET) method to investigate the homodimerization mechanism and intradimer molecular interactions in endophilin. For the endophilin N-BAR domain (which lacks the SH3 domain including a linker region of the full length protein), we observe a large temperature dependence of the dimerization affinity and dimer dissociation kinetics, implying large dimerization enthalpy and dissociation activation enthalpy, respectively. Our evaluation of the protein concentration dependence of dimer dissociation kinetics implies that endophilin reversibly forms monomers via a dissociation/reassociation mechanism. Furthermore, we use a kinetic method that allows us to compare the dissociation kinetics of full-length endophilin to that of truncated mutants. We find that mutants that lack either H0 helix or SH3 domain show significantly faster dissociation kinetics relative to full-length endophilin. This observation supports the presence of an intradimer, intermonomer cross-interaction between H0 helix and SH3 domain from different subunits within a homodimer. Because the H0 helix is known to play a significant role in endophilin's membrane interactions, our measurements support a syngergistic model where these interactions are inhibited in the absence of SH3 domain binding ligands such as dynamin's prolin rich domains, and where the binding of these ligands may be suppressed for non-membrane-bound endophilin.

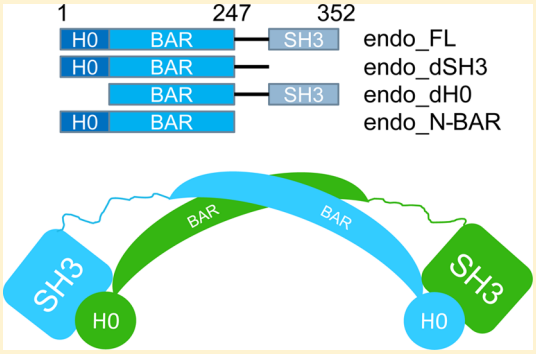

INTRODUCTION

Endophilin, a peripherally binding membrane protein, functions in multiple membrane trafficking processes that involve changes in membrane curvature.[1−5] The function of this protein includes both membrane curvature sensing,[6,7] and curvature generation.[8] Endophilin consists of an N-terminal amphipathic helix (H0), a Bin-Amphiphysin-Rvs (BAR) domain, a SRC Homology 3 (SH3) domain, and a flexible linker to connect BAR domain and the SH3 domain (Figure 1A).[9] The BAR domain is known to mediate the dimerization of endophilin.[9−11] The mechanism of endophilin's function is believed to depend, at least in part, on the effect of scaffolding through the crescent shape of the protein (Figure 1B).[12−15] The shape of endophilin's membrane binding interface depends on its dimeric structure.[10,11] Therefore, knowledge of the thermodynamics of endophilin dimerization is crucial to understand the function of the protein. The SH3 domain of endophilin recruits dynamin and synaptojanin.[3,16,17] However, the role of the SH3 domain in clathrin-mediated endocytosis (CME) is not yet fully understood. For example, Bai et al.[5] reported that the endocytic function of endophilin is independent of the SH3 domain, while Milosevic et al. reached opposing conclusions.[18] Vazquez et al.[19] have performed molecular-dynamics (MD) simulations to study properties of a hypothesized H0-SH3 complex in solution and proposed an autoinhibition model where the SH3 domain and H0 helix from the same subunit form a complex through hydrophobic and salt-bridge interactions. This autoinhibition model is in agreement with a previous study based on small-angle X-ray scattering (SAXS), which suggested that each SH3 domain is best fitted when assumed to be localized near the distal end of the N-BAR dimer, where the H0 helix is located.[20] Finally, Meinecke et al. reported that the membrane binding of endophilin is autoinhibited when dynamin is absent

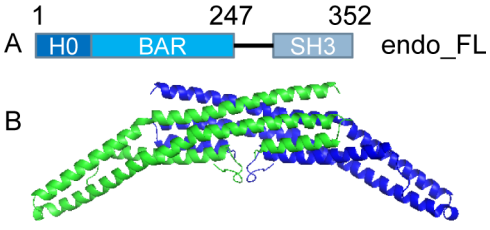

Figure 1. (A) Domain structure of full-length rat endophilin A1. (B) Crescent shape of dimeric endophilin BAR domain (PDB: 2C08).

Received: November 14, 2013
Published: February 25, 2014

   dx.doi.org/10.1021/ja411607b | J. Am. Chem. Soc. 2014, 136, 4557−4564

from solution.[21] However, little experimental evidence for an H0-SH3 based autoinhibition mechanism has been reported. We fill this gap via measurements of endophilin dimer dissociation kinetics.

Kinetic characterization of protein/protein association has commonly been performed via techniques such as subunit cross-linking,[22,23] size exclusion chromatography,[24] or spectroscopic techniques.[25−28] Surface plasmon resonance represents an alternative kinetic technique, although its limitations in kinetic studies of protein association have been discussed.[29] Subunit exchange with detection by Förster resonance energy transfer (FRET) circumvents many of the challenges associated with applying the above-mentioned approaches to the study of homodimers.

Our previous subunit exchange FRET studies of the endophilin N-BAR (endo_N-BAR) domain at one single temperature reported subnanomolar dimerization affinity.[30] This affinity, far higher than that reported previously using analytical ultracentrifugation,[9] was rationalized by the correlation between dimer interface area and dimerization affinity.[31] Endo_N-BAR exhibits large dimer interface area compared to many other protein−protein complexes of known affinities as tabulated in ref 32.

In this contribution we develop a model for molecular interactions in the full length endophilin protein dimer in two steps. We first focus on endophilin's N-BAR domain to illuminate the physicochemical basis for the strong dimerization affinity of endophilin. We extend our previous kinetic and thermodynamic investigation of endo_N-BAR to a range of different temperatures to provide a basis for a mechanistic discussion of endo_N-BAR dimer dissociation. We discuss the contributions of various classes of molecular interactions to the stability of endo_N-BAR dimers and elucidate the mechanism of the endo_N-BAR monomer exchange reaction. Furthermore, to investigate molecular interactions in the full length protein (endo_FL), we develop a kinetic method that allows us to reveal significant differences in dissociation kinetics for endo_FL relative to endo_N-BAR. Mutants lacking either H0 helix (endo_dH0) or SH3 domain (endo_dSH3) showed significantly faster dissociation kinetics relative to endo_FL. This observation is consistent with an intradimer, intermonomer cross-interaction of H0 helix and SH3 domain from different subunits of the same homodimer in solution. We finally propose a model for intradimer autoinhibition that is based on this cross-interaction.

MATERIALS AND METHODS

We used FRET as an approach to monitor the subunit exchange kinetics and to probe the equilibrium binding affinity of endophilin A1 in solution. Endophilin was cysteine labeled with Pacific Blue or Alexa 488 at position 241 to create a donor/acceptor FRET pair. Monomer exchange kinetics was monitored (except where indicated otherwise) after mixing differently labeled proteins while maintaining a constant overall protein concentration. Equilibrium binding affinity was measured after equilibrating mixed differently labeled proteins with varied concentrations. The data analysis of the kinetics results used previously established protocols.[30,33,34] The method we used to quantify sensitized emission in the mixed sample at equilibrium, and to relate it to the dimerization affinity, is closely related to the Em-ex method described in the literature.[35,36]

Additional information on materials and methods are available in the Supporting Information (SI).

RESULTS

Two-State Dimerization Model. Several kinetic schemes have been proposed to describe protein−protein association processes. A four-state model, including experimentally observed encounter and intermediate complex, was reviewed by Schreiber.[37] However, for some cases, the association process has been shown to follow a three-state or two-state scheme.[37]

The investigation of the dependence of protein/protein dissociation (and association) kinetics on denaturant concentration can yield important information on the mechanism of the reaction. Therefore, we use a kinetic FRET method to determine the dissociation rate constant, k_{off}, for endo_N-BAR as a function of urea concentration at 27 °C (see SI for details). As shown in Figure 2, kinetic measurements of endo_N-BAR monomer exchange revealed a linear trend of $\log(k_{off})$ as a function of denaturant concentration. This suggests that endo_N-BAR homodimer dissociation occurs through a two-state process in which monomers and dimers are the only two significantly populated species.[34,38] In the following, we therefore interpret all experiments based on the two-state hypothesis and provide additional justification for this hypothesis below.

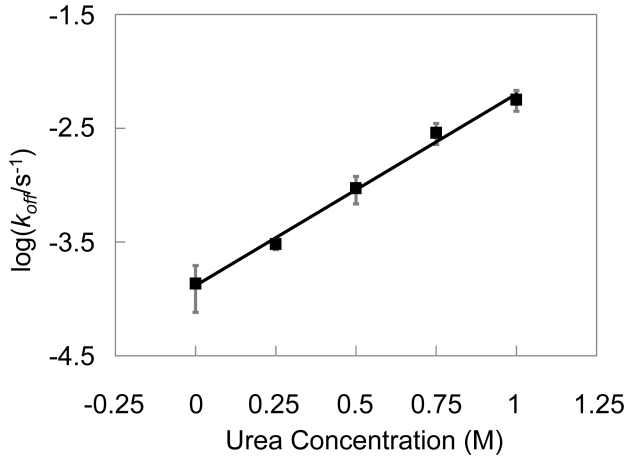

Figure 2. Kinetic test of two-state dimer dissociation/monomer association by adding the denaturant urea. A plot of $\log(k_{off})$ vs urea concentration revealed a linear trend. Error bars: standard error of the mean.

Temperature Dependence of Endo_N-BAR Dissociation Kinetics. We used a FRET approach that involved mixing two protein samples, each labeled separately with donor and acceptor, respectively, and monitoring increased FRET through subunit exchange (for details see SI). By fitting these kinetic FRET data, we determined k_{off} for endo_N-BAR dimer dissociation at different temperatures to extract activation parameters. We note that it can be shown analytically that the subunit exchange kinetics monitored here via FRET are indeed expected to be independent of the on-rate of monomer association.[22] Figure 3A summarizes the results of these kinetic measurements. As shown in Figure S2D (SI), the FRET efficiency time traces were well fitted by a single exponential function (eq S2 (SI)). The first-order nature of the dissociation process supports our two-state hypothesis. Measurements were carried out at temperature ranging from 22 to 37 °C (see Table 1). The dissociation rate constant, k_{off}, ranged from 3×10^{-5} s^{-1} at 22 °C to 6×10^{-3} s^{-1} at 37 °C.

dx.doi.org/10.1021/ja411607b | J. Am. Chem. Soc. 2014, 136, 4557−4564

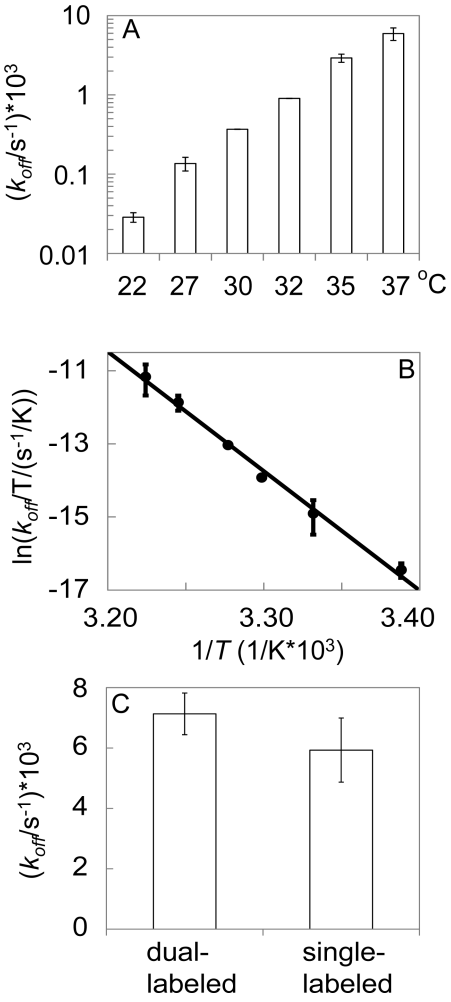

Figure 3. Temperature dependence of dissociation rate constant for endo_N-BAR by FRET. (A) k_{off} values ranged from 3×10^{-5} s^{-1} at 22 °C to 6×10^{-3} s^{-1} at 37 °C. (B) $\ln(k_{off}/T)$ follows a linear trend with respect to $1/T$, which corresponds to the linear form of the Eyring–Polanyi equation, eq 1. Intercept and slope report activation enthalpy of 66 kcal/mol and activation entropy of 140 cal/mol/K. (C) Comparison of averaged k_{off} values obtained from two different kinetic measurements (k_{off} value obtained from mixing dual-labeled proteins with unlabeled proteins and that from mixing two single-labeled proteins). Error bars (standard error of the mean) for each data point were calculated from at least three trials for each sample.

The bar graphs in Figure 3 show average values from at least three trials for all the temperature points except for 22 °C, where measurements demand roughly 40 h, and two trials with sufficient agreement were collected (potential protein misfolding and hydrolysis were excluded on the basis of circular dichroism spectra and gel electrophoresis for samples incubated at room temperature for this duration, data not shown). An increase in the endo_N-BAR dissociation rate constant was observed with increasing temperature. $\ln(k_{off}/T)$ follows a linear trend with respect to $1/T$ in the temperature range from 22 to 37 °C (Figure 3B). To interpret measured reaction rate constants, several rate theories have been developed. The theories that have been most widely applied to biological systems are due to Eyring, Kramers, and Smoluchowski, respectively.[39] Here, we use the Eyring–Polanyi theory to interpret the endo_N-BAR dimer dissociation process:[39,40]

$$\ln\left(\frac{k_{off}}{T}\right) = -\frac{\Delta H^{\ddagger}}{RT} + \ln\left(\frac{k_B}{h}\right) + \frac{\Delta S^{\ddagger}}{R} \quad (1)$$

where k_B is the Boltzmann constant, h is Planck's constant, R is the ideal gas constant, T is absolute temperature, $\Delta H^{\ddagger}$ is enthalpy of activation, and $\Delta S^{\ddagger}$ is entropy of activation. The activation enthalpy and entropy of endo_N-BAR dimer dissociation are thus obtained from the slope, $-(\Delta H^{\ddagger}/R)$, and intercept, $\ln(k_B/h) + (\Delta S^{\ddagger}/R)$, of the linear fit, leading to an activation enthalpy of 66 kcal/mol and an activation entropy of 140 cal/mol/K.

Temperature points lower than room temperature or higher than 37 °C were not considered because of two limitations: when temperature is lower than room temperature, long equilibration times (approximately 1 month at 15 °C, and 9 years for 4 °C; from extrapolation) are needed for a single kinetic measurement. For temperatures higher than 40 °C, reactions will equilibrate in a very short time (approximately 3 min at 42 °C). Consequently, the initial FRET would overestimate that of a nonexchanged mixture.

The potentially artifactual effect of dye labeling on the kinetics of endo_N-BAR dimerization/dissociation was evaluated by comparing the results obtained from two different kinetic measurements at the same temperature: monitoring the kinetics of mixing dual-labeled protein with unlabeled protein and the kinetics of mixing two single-labeled protein samples (see Figure S2E,F (SI)). The results are shown in Figure 3C, where values for the dual-labeled sample are averaged from three measurements, and those for the single-labeled sample are averaged from five measurements.

A Student t-test yielded a t-value of $t_{cal} = 0.95$, corresponding to $P > 0.05$, and thus no significant difference was observed for the kinetics of labeled and unlabeled endo_N-BAR domains. We conclude that it is unlikely that the labels on endo_N-BAR alter the kinetics of protein dimerization and dissociation or perturb the equilibrium between endo_N-BAR dimers and monomers.

Temperature Dependence of Endo_N-BAR Equilibrium Dimerization Affinity. In order to determine the dimerization affinity of endo_N-BAR, equilibrated samples were used for FRET measurements (see SI). Figure 4 shows an

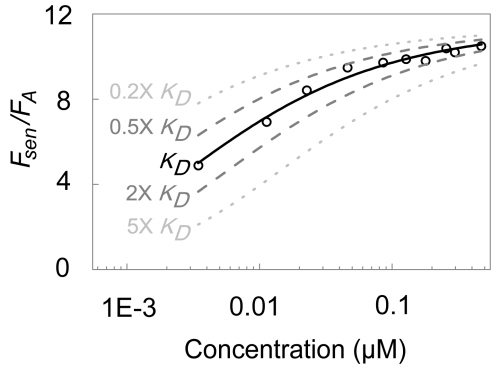

Figure 4. Comparison of equilibrium dimerization affinity measurements and fitting. Samples of 10 different concentrations with the same D/A ratio were incubated and measured at 37 °C. Open circles represent experimentally determined (F_{sen}/F_A) values. Fitting with eq S9 (SI) yields the black solid curve shown, with parameters, $A = 11.4$ and $K_D = 4.89$ nM. Dotted and dashed gray curves from top to bottom represent fitting results with K_D values 5-fold smaller, 2-fold smaller, 2-fold larger and 5-fold lager, respectively.

dx.doi.org/10.1021/ja411607b | J. Am. Chem. Soc. 2014, 136, 4557–4564

example of measurements at 37 °C of fluorescence due to sensitized emission (F_{sen}), relative to fluorescence due to direct excitation of the acceptor (F_A). (F_{sen}/F_A) values determined over a range of protein concentrations were fitted by eq S9 (SI), yielding K_D = 4.89 nM (Figure 4 black solid curve).

To test the reliability of the fitting of the experimental data, we compared to the fit result theoretical titration curves that assumed 2-fold or 5-fold larger or smaller K_D values. These are shown as gray dotted or dashed curves in Figure 4. This comparison shows that the determined K_D value is reliable, since the range of alternative K_D values considered leads to a substantial deviation from the experimental measurements.

The temperature dependence of the dimerization affinity was observed from measurements at five temperatures. 27 °C was chosen as the lowest temperature that allowed reliable FRET titrations. Figure 5A summarizes our measurements of the

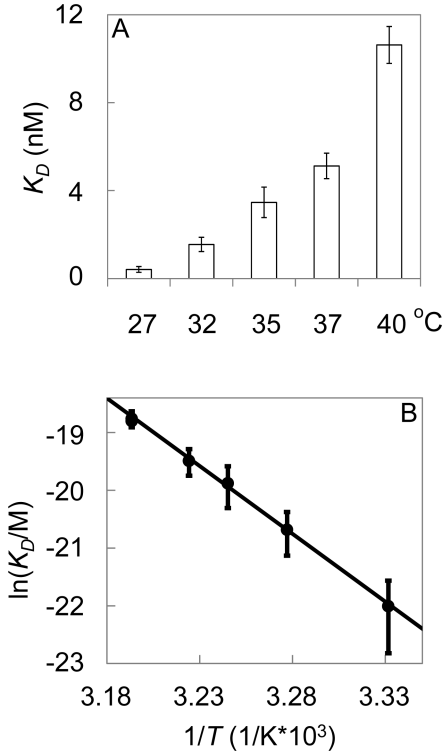

Figure 5. Temperature dependence of dimerization affinity for endo_N-BAR by FRET. (A) K_D values exhibit a change of greater than 20-fold between 27 and 40 °C. All temperature points are averaged from at least three trials. (B) ln K_D follows a linear trend with respect to $1/T$, which corresponds to the linear form of the Van't Hoff equation, eq 2. Intercept and slope of the linear plot yield dissociation equilibrium enthalpy change of 47 kcal/mol and entropy change of 112 cal/mol/K. Error bars: standard error of the mean.

dimer dissociation equilibrium constant, K_D, which ranges from 0.4 nM at 27 °C to 11 nM at 40 °C, confirming our earlier affinity assessment at a single temperature.[30] In Figure 5B, a plot of the natural logarithm of the equilibrium constant versus the reciprocal temperature yields a straight line, which is expected from the Van't Hoff equation,[40]

$$\ln K_D = -\frac{\Delta H}{RT} + \frac{\Delta S}{R} \qquad (2)$$

where ΔH and ΔS are the equilibrium enthalpy and entropy change of the reaction. Via eq 2, we obtain an equilibrium enthalpy change of 47 kcal/mol and equilibrium entropy change of 112 cal/mol/K.

The above measurements provided the temperature-dependent N-BAR dimer dissociation rate constants and equilibrium dimer dissociation constants. Association rate constants, k_{on}, were determined from the ratio of k_{off} and K_D, which is appropriate for a two-state reaction mechanism. Table 1 lists

Table 1. List of Experimental and Predicted Thermodynamic Parameters[a,b]

temperature (°C)	k_{off} (s^{-1})	k_{on} (M^{-1} s^{-1})	K_D (M)	ΔG (kcal/mol)
4	*1.7×10^{-8}*	*2.5×10^{4}*	*6.8×10^{-13}*	*15.4*
27	1.5×10^{-4}	3.7×10^{5}	4.2×10^{-10}	11.9
32	9.3×10^{-4}	6.3×10^{5}	1.5×10^{-9}	11.2
35	2.7×10^{-3}	8.6×10^{5}	3.1×10^{-9}	10.8
37	5.3×10^{-3}	1.1×10^{6}	5.1×10^{-9}	10.5

[a] k_{on} values at different temperatures are calculated from K_D and k_{off}. [b] Values that are displayed in italic font (at 4 °C) resulted from extrapolation of the linear trends found in Figure 3 and Figure 5.

experimental and predicted thermodynamic parameters, k_{off}, K_D, and the calculated k_{on} values at five different temperatures. An Arrhenius plot of these data allows calculation of the association activation enthalpy (see Figure S4 (SI)).

As described above, the dimer dissociation requires an activation enthalpy of 66 kcal/mol and results in an equilibrium enthalpy change of 47 kcal/mol. The activation entropy for dissociation is 140 cal/mol/K, with an equilibrium entropy change of 112 cal/mol/K (Table 2).

Table 2. Summary of Equilibrium Reaction Enthalpies and Entropies, As Well As Activation Values for Association and Dissociation, Respectively[a]

	enthalpy (kcal/mol)	entropy (cal/mol/k)	free energy (kcal/mol)
dissociation (activation)	66	140	24
association (activation)	19	28	10.7
dissociation (equilibrium)	47	112	13.4

[a] Gibbs free energy values were calculated on the basis of the enthalpy and entropy values at 25 °C.

We note that, thus far, we have performed all of our measurements at the same total protein concentration of 2 μM. The choice of this single concentration is indeed justified, because kinetic measurements for different concentrations show no significant changes in protein dissociation kinetics over the concentration range of 0.1 to 3 μM (Figure 6). As we discuss below, this finding has important bearing on the dissociation/reassociation mechanism of the endo_N-BAR monomer exchange reaction.

Dissociation Kinetics of Full-Length Endophilin. Kinetic FRET measurements were carried out to delineate the dimerization difference between endophilin N-BAR and full-length protein. Distinct dissociation kinetics between endo_N-BAR and endo_FL were revealed. For endo_N-BAR, donor quenching was observed to equilibrate within about 10 min at 37 °C, Figure 7A). In sharp contrast to the behavior of endo_N-BAR, no significant time dependence of

dx.doi.org/10.1021/ja411607b | J. Am. Chem. Soc. 2014, 136, 4557−4564

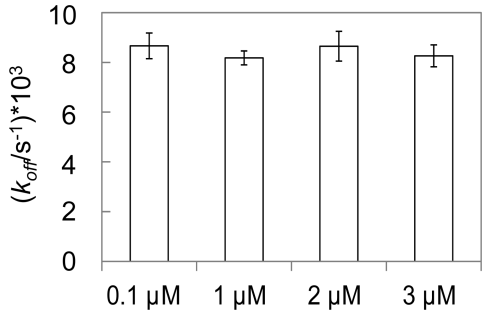

Figure 6. Absence of concentration dependence for dimer dissociation rate constants. All measurements were carried out as described above, at 37 °C. Error bars: standard error of the mean.

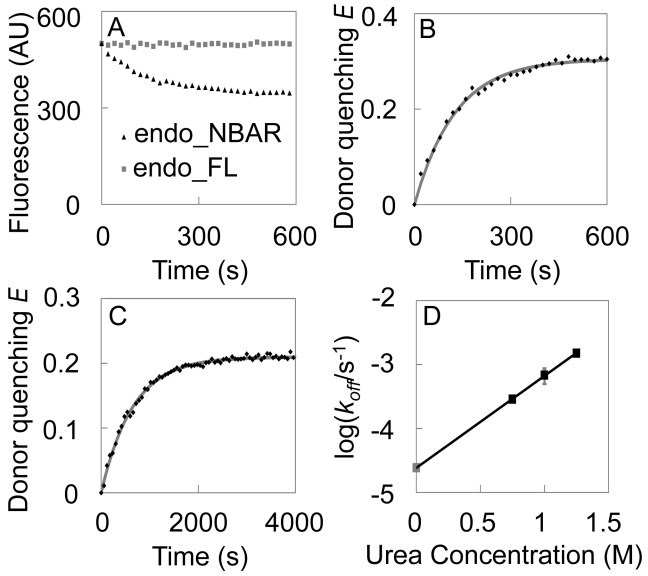

Figure 7. Kinetic measurements to determine dimer dissociation rate constant. (A) At 37 °C, donor quenching was observed for endo_N-BAR but not for endo_FL in 10 min. (B) FRET efficiency of endo_N-BAR shown in (A) was calculated according to eq S1 (SI), and time traces were well fitted by eq S2 (SI) (gray solid line), yielding k_{off} = 7.88×10^{-3} s^{-1}, E_{inf} = 31%. (C) At 37 °C, the FRET efficiency trace of a kinetic measurement of endo_FL in buffer solution with 1.25 M urea can be well fitted by eq S2 (SI), yielding k_{off} = 1.54×10^{-3} s^{-1}, E_{inf} = 21%. (D) At 37 °C, summary of kinetic measurements of full-length endophilin with three urea concentrations, 0.75, 1, 1.25 M, respectively. All data points are averages from three trials, and the bars are standard errors of the mean. $\log(k_{off}/s^{-1})$ shows a linear change with respect to urea concentration. The dissociation rate constant, k_{off}, at zero urea condition was obtained by linear extrapolation to be $(2.4 \pm 0.21) \times 10^{-5}$ s^{-1}, which is 244-fold slower than that of endo_N-BAR.

the donor signal was observed for endo_FL within 10 min (Figure 7A). This comparison suggests that the rate of homodimer dissociation for endo_FL is far slower than that of endo_N-BAR and cannot be detected within 10 min.

We therefore used the protein denaturant urea to accelerate subunit exchange for endo_FL. As Figure 7C shows, this resulted in accelerated FRET efficiency changes that were well fitted by a single exponential. As for endo_N-BAR, the investigation of the dependence of protein dissociation (and association) kinetics on denaturant concentration revealed a linear trend of $\log(k_{off})$ as a function of denaturant concentration (Figure 7D). Thus, the dissociation rate constant k_{off} for endo_FL was obtained from linear extrapolation to zero urea concentration as 2.4×10^{-5} s^{-1}, which is over 200-fold slower than that of endo_N-BAR, as determined above. We note that the observations of (a) single-exponential kinetics of endo_FL FRET efficiency traces and (b) the linear dependence of $\log(k_{off})$ on denaturant concentration are in accordance with the hypothesis of an effective two-state mechanism for the endo_FL monomer/dimer equilibrium, as we argued for endo_N-BAR.

Dissociation Kinetics of Endophilin Mutants. We next aimed to evaluate possible mechanisms behind the differing dissociation rate constants comparing endo_FL and endo_N-BAR. Structurally, the difference between endo_FL and endo_N-BAR is the flexible linker and the SH3 domain. Therefore, intradimer interactions between the H0 helix and the SH3 domain, interactions between the BAR domains and the SH3 domains, H0/H0 helix as well as SH3/SH3 domain interactions, and interactions between linkers and SH3 domains all might contribute to the far slower dissociation kinetics observed for endo_FL. The interaction between the H0 helix and SH3 domain can be considered the most likely alternative interaction resulting in the deceleration of endo-FL dissociation, since previous SAXS[20] and MD simulation[19] studies have provided support for this interaction.

To test the hypothesis that the difference in dissociation kinetics for endo_FL relative to endo_N-BAR is caused by an H0-SH3 interaction, two additional fluorescently labeled mutants (endo_dSH3 and endo_dH0) were designed. As shown in Figure 8A, endo_dSH3 is a mutant consisting of the N-BAR domain and the flexible linker but missing the SH3 domain, and endo_dH0 is a mutant of endo_FL that is lacking the H0 helix. These two mutants were also subjected to kinetic analysis to determine their dissociation rate constants. The average values and standard errors of the dissociation rate constants obtained for endo_N-BAR, endo_dSH3, endo_dH0 and endo_FL are plotted in Figure 8B. Mutants lacking either H0 helix or SH3 domain exhibit significantly faster (176- and 191-fold) dissociation kinetics than endo_FL. These observations are consistent with the notion that the copresence of H0 helix and SH3 domain hinders the dissociation of endo_FL, and inconsistent with a significant role of the linker, or any SH3/BAR domain interactions, in intradimer endophilin interactions that would slow dimer dissociation.

■ DISCUSSION

Dimer Dissociation Mechanism. We have interpreted our measurements of endo_N-BAR dissociation kinetics in the framework of a scheme that assumes dissociation of dimers followed by reassociation of two monomers to form a dimer. Two alternative mechanisms for monomer exchange in endophilin dimers might be envisioned that would also display the single exponential kinetics that we observed (Figure 7B,C and Figure S2 (SI)).[22] These are (a) dissociation of a dimer into monomers, followed by attack of a monomer on a dimer resulting in a displacement, and (b) collision of two dimers followed by monomer exchange. It is clear, however, that both of these alternative mechanisms would result in a concentration dependence of the (in those cases apparent) first-order rate constant for dissociation,[22] which we did not observe (see Figure 6).

The dissociation−reassociation mechanism (that is consistent with our observations) for endo_N-BAR monomer exchange implies that endo_N-BAR reversibly forms mono-

dx.doi.org/10.1021/ja411607b | J. Am. Chem. Soc. 2014, 136, 4557−4564

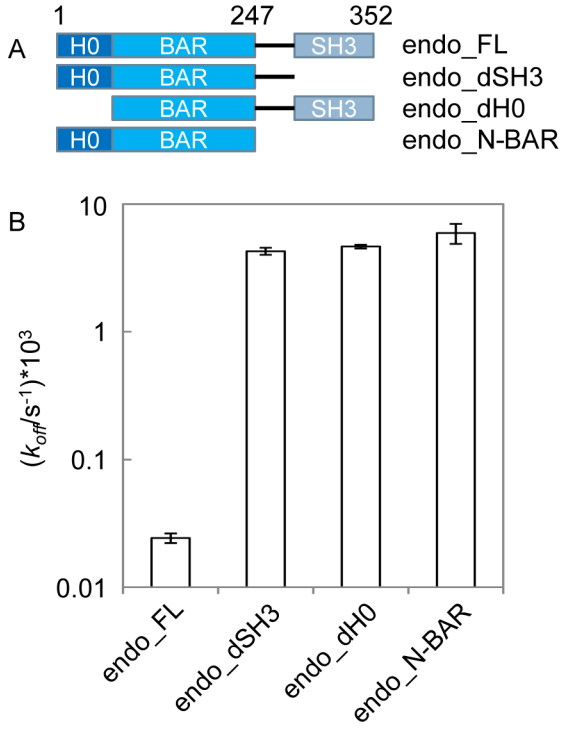

Figure 8. (A) Domain structure of full-length endophilin (endo_FL), as well as of three mutants: endo_dSH3, endo_dH0, and endo_N-BAR. The black bar connecting SH3 and BAR domains is a flexible unstructured linker sequence. (B) Comparison of dissociation rate constants among endo−FL and its mutants. The obtained dissociation rate constants reveal faster dimer dissociation kinetics for the mutants compared to full-length endophilin A1. The dissociation rate constant ratio is 1:(176 ± 12):(191 ± 6):(244 ± 44) from left to right. Error bars: standard error of the mean.

mers. This means that (at least under our in vitro conditions) endophilin monomers are sufficiently stable to prevent irreversible unfolding of the monomer. This result might imply a biological relevance of the monomeric form of endophilin as has been suggested before.[5] However, the nano- to subnanomolar affinities determined here and previously[30] of endo_N-BAR dimerization at physiological temperature tend to disfavor a physiological role for monomeric endo_N-BAR, as we have argued before.[30]

Support for Two-State Hypothesis. Our two-state hypothesis for the kinetics of endophilin dissociation is based on the following three observations: (a) denaturation experiments reveal a linear trend of $\log(k_{off})$ versus denaturant concentration[34,38] (Figure 2 and Figure 7D); (b) exchange kinetics are well described by first-order reaction kinetics for the dissociation reaction that follow a temperature dependence in line with the Eyring−Polanyi theory[39,40] (Figure 3B, Figure 7B,C, and Figure S2 (SI)); and (c) equilibrium titration FRET measurements could be well fitted with a two-state model (Figure 4, eq S9 (SI)).

Thermodynamics of Endophilin Dimerization. The temperature dependence of the equilibrium titration FRET measurements revealed that endo_N-BAR homodimer dissociation is associated with both positive reaction enthalpy and entropy (Table 2). This indicates that despite the presence of a large hydrophobic patch in the dimerization interface,[9] the dimer is not predominantly stabilized by hydrophobic interactions. Instead, it is likely that a combination of van der Waals interactions, hydrogen bond formations, and salt bridge formations overcompensates contributions from hydrophobic interactions to dimer stability.[41] Indeed, for the endo_N-BAR dimer, 16 interfacial H-bonds (HB) and 8 salt bridges (SB) were identified using the PISA (Protein Interfaces, Surfaces and Assemblies) server.[42] The disruption of intermolecular H-bonds during dimer dissociation would yield a free energy change of 0.6−1.5 kcal/mol per bond, and salt bridges have similar free energy contributions to the dissociation reaction.[42] Therefore, these interactions likely significantly contribute to endo_N-BAR dimer stabilization. We note that PISA yields an overall solvation free energy change for the dissociation reaction of endo_N-BAR of 43.9 kcal/mol.[42] The difference of this value to our measured value of 13.4 kcal/mol at 25 °C (Table 2) is likely explained by the many simplifications[42] implied in the PISA method of calculating thermodynamic aspects of protein multimerization. PISA indicates a value of $T * \Delta S_{diss}$ to be 13.8 kcal/mol, which is smaller than our measured value of 33.6 kcal/mol at 25 °C. The discrepancy is possibly explained by the neglect of vibrational entropy changes arising from the formation of new modes in the complex in place of degrees of freedom that get restricted by association.[42] The experimentally measured thermodynamic parameters of endo_N-BAR compare well to other homodimeric proteins that have somewhat similar interface characteristics. For example, the buried interface area of the HIV-1 protease homodimer (PDB: 1hxw) is 1718.7 Å^2 (via PISA) per subunit and is predicted to contain 22 HBs and 7 SBs. The reported Gibbs free energy for HIV-1 protease homodimer dissociation (12 kcal/mol[43,44]) and unfolding (14.4 kcal/mol[45]) are close to the value for endo_N-BAR homodimer dissociation (Table 2). Another example is Arc repressor (PDB: 1arr). The reported dissociation and unfolding Gibbs free energy is ∼10 kcal/mol[34,43] for the Arc homodimer, which is somewhat comparable with endophilin N-BAR, likely due to the related characteristics of the buried interface (an area of 1958.3 Å^2 with 31 HB and 2 SB that are predicted by PISA for the Arc repressor).

We found an activation enthalpy for endo_N-BAR association of 19 kcal/mol (Table 2), which was determined on the basis of the assumption of a two-state dimerization reaction. This value indicates that the endo_N-BAR association reaction is not a simple diffusion-controlled reaction. The activation energy (which differs from activation enthalpy by about 0.6 kcal/mol) for self-diffusion of water is 4.6 kcal/mol.[46,47] For oligomerizing proteins with charged amino acids, the diffusion limit for multimer formation kinetics is significantly influenced by electrostatic interactions.[29] Association rate constants in the diffusion limited regime, where association kinetics is dominated by the diffusion time required to form a transient complex, can be calculated using the TransComp server.[48] For reaction kinetics that are controlled by the formation of the transient complex (where short-range native interactions can be neglected), TransComp allows for the calculation of the diffusion limited association rate constant, as well as an electrostatic interaction energy for protein association. Through TransComp, the electrostatic interaction energy for endo_N-BAR association is determined to amount to 2.384 kcal/mol. This result indicates that the electrostatic energy contributes positively to the positive activation energy of endo_N-BAR association. Interestingly, the electrostatic interactions between the two associating subunits therefore disfavor subunit association and thus slow down the association

dx.doi.org/10.1021/ja411607b | J. Am. Chem. Soc. 2014, 136, 4557−4564

process. The electrostatic contribution, however, is less than a quarter of the activation Gibbs free energy required for endo_N-BAR association (Table 2). As a consequence of the different activation energies, the calculated association rate constant (2.24×10^2 M^{-1} s^{-1}) using TransComp is far smaller than the experimental values determined above. This discrepancy likely can be ascribed to the assumptions implicit in the TransComp calculation, such as the rigid body assumption.[48] Therefore, our findings suggest that endo_N-BAR monomers undergo significant molecular rearrangements during dimer formation.

Intradimer Cross-Interaction. Our next aim was to test the hypothesis of a binding interaction between H0 helix and SH3 domain. We eliminated interactions between endophilin BAR domain and the SH3 domain as a likely intradimer interaction since no obvious interaction was indicated by RosettaDock[49,50] (not shown here). The interactions between the SH3 domain and the N-BAR domain or flexible linker can be deemed unlikely on the basis of our experimental findings (Figure 8B), and additionally on the grounds that a publicly accessible "SH3 hunter" server,[51] which identifies SH3 domain interaction sites in proteins, failed to reveal a sequence matching the SH3 consensus. Mim et al.[52] proposed interactions between H0 domains from different homodimers on the membrane; however, we have previously excluded higher oligomer formation of endo_N-BAR in solution.[30]

Vazquez et al. predicted formation of an H0-SH3 complex within the same monomer of the endophilin dimer.[19] This model, however, cannot explain the substantially slowed dissociation kinetics observed for full-length relative to N-BAR endophilin. The kinetic comparison shown in Figure 8B shows that mutants lacking either H0 helix or SH3 domain exhibit significantly faster (176- and 191-fold) dissociation kinetics than endo_FL. This observation is consistent with the notion that the copresence of H0 helix and SH3 domain hinders the dissociation of endo_FL and led us to propose a modified model where the SH3 domain cross-interacts with the H0 helix from a different subunit within a single dimer in solution (Figure 9). This model is consistent with a solution-phase small-angle X-ray scattering (SAXS) study, which suggested that each SH3 domain is best fitted when assumed to be located near the distal end of the N-BAR dimer.[20] It is conceivable that the H0/SH3 domain cross-interaction, as in the model proposed in Figure 9, results in an increased barrier for endophilin homodimer dissociation and, hence, slower dissociation kinetics. Furthermore, Figure 8 shows that the kinetics of endo_dSH3 and endo_dH0 mutants are close to that of endo_N-BAR, which is consistent with our model since the retardation of dimer dissociation is released when either the H0 domain or the SH3 domain is absent in the mutant.

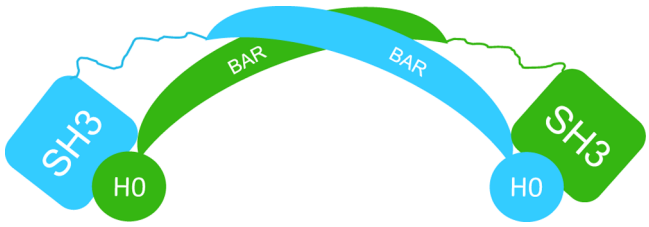

Figure 9. SH3-H0 cross-interaction mechanism. Cartoon to illustrate the intradimer intermonomer SH3-H0 cross-interaction.

Consistent with our model, Vazquez et al. proposed that the H0-SH3 complex likely implies that the H0 helix can be stabilized in solution through the H0/SH3 cross-interaction.[19] Because of the formation of this complex, a syngergistic autoinhibition mechanism can be expected: (a) the H0 helix is inhibited from inserting into the membrane in the absence of SH3 binding ligands, and (b) the SH3 domain will be inhibited from interacting with other proteins such as dynamin's prolin rich domain for non-membrane-bound endophilin.[19] In keeping with this expectation, addition of dynamin leads to a significant increase of endophilin binding to model membranes.[21] This experimental finding is consistent with the notion that the presence of SH3 binding ligands can be essential for the release of H0-SH3 mediated autoinhibition of endophilin. We have confirmed this finding by comparing the membrane binding capacity of endo_FL, endo_N-BAR, endo_dSH3, and endo_dH0 under identical experimental conditions (Figure S5 (SI)). We observed lower membrane binding intensity for endo_FL than for endo_N-BAR, supporting an autoinhibition of the full length protein.

CONCLUSIONS

In this contribution we have determined the temperature dependence of endophilin N-BAR dimerization kinetics and thermodynamics. Over the temperature range considered, low nanomolar to subnanomolar affinities were found, and positive dimer dissociation enthalpy and entropy were interpreted as subdominance of hydrophobic contributions to dimerization thermodynamics. Large dimer dissociation and association activation enthalpies were interpreted as potentially indicating significant conformational rearrangement during dissociation/reassociation reactions. The absence of a protein concentration dependence on dimer dissociation kinetics allowed us to rule out dimer dissociation mechanisms alternative to a dissociation/reassociation mechanism.

Furthermore, we have developed a kinetic method that allowed us to test intradimer/intermolecular interactions that illuminate a hypothesized autoinhibition mechanism. We found experimental evidence for an H0/SH3 interaction within full-length endophilin in solution, suggesting a model where the SH3 domain and the H0 helix from different subunits in a homodimer engage in a cross-interaction. The SH3/H0 cross-interaction slows down the kinetics of dimer dissociation and is thus expected to enhance the dimerization affinity of full-length endophilin homodimers relative to the BAR domain. In summary, this contribution, through kinetic and equilibrium FRET studies, illustrates the physicochemical basis for the high binding affinity of the endophilin N-BAR domain and illuminates the role of the SH3 domain in full-length endophilin's autoinhibition mechanism in solution.

ASSOCIATED CONTENT

Supporting Information

Additional materials and methods; linear plot of natural logarithm of the association rate constant with respect to the reciprocal temperature. This material is available free of charge via the Internet at http://pubs.acs.org.

AUTHOR INFORMATION

Corresponding Author

baumgart@sas.upenn.edu

Notes

The authors declare no competing financial interest.

■ ACKNOWLEDGMENTS

We acknowledge funding from National Institutes of Health Grant R01GM097552. We thank Drs. Saven and Park for access to their fluorimeters and Dr. Gai and Chun-Wei Lin for access to their Circular Dichroism instrument.

■ REFERENCES

(1) Ringstad, N.; Gad, H.; Low, P.; Di Paolo, G.; Brodin, L.; Shupliakov, O.; De Camilli, P. *Neuron* **1999**, *24*, 143.
(2) Llobet, A.; Gallop, J. L.; Burden, J. J. E.; Camdere, G.; Chandra, P.; Vallis, Y.; Hopkins, C. R.; Lagnado, L.; McMahon, H. T. *J. Neurosci.* **2011**, *31*, 8512.
(3) Sundborger, A.; Soderblom, C.; Vorontsova, O.; Evergren, E.; Hinshaw, J. E.; Shupliakov, O. J. *Cell Sci.* **2011**, *124*, 133.
(4) Ferguson, S.; Raimondi, A.; Paradise, S.; Shen, H. Y.; Mesaki, K.; Ferguson, A.; Destaing, O.; Ko, G.; Takasaki, J.; Cremona, O.; O'Toole, E.; De Camilli, P. *Dev. Cell.* **2009**, *17*, 811.
(5) Bai, J. H.; Hu, Z. T.; Dittman, J. S.; Pym, E. C. G.; Kaplan, J. M. *Cell* **2010**, *143*, 430.
(6) Zhu, C.; Das, S. L.; Baumgart, T. *Biophys. J.* **2012**, *102*, 1837.
(7) Bhatia, V. K.; Madsen, K. L.; Bolinger, P. Y.; Kunding, A.; Hedegard, P.; Gether, U.; Stamou, D. *EMBO J.* **2009**, *28*, 3303.
(8) Farsad, K.; Ringstad, N.; Takei, K.; Floyd, S. R.; Rose, K.; De Camilli, P. J. *Cell. Biol.* **2001**, *155*, 193.
(9) Gallop, J. L.; Jao, C. C.; Kent, H. M.; Butler, P. J. G.; Evans, P. R.; Langen, R.; T McMahon, H. *EMBO J.* **2006**, *25*, 2898.
(10) Masuda, M.; Mochizuki, N. *Semin. Cell Dev. Biol.* **2010**, *21*, 391.
(11) Peter, B. J.; Kent, H. M.; Mills, I. G.; Vallis, Y.; Butler, P. J. G.; Evans, P. R.; McMahon, H. T. *Science* **2004**, *303*, 495.
(12) Boucrot, E.; Pick, A.; Camdere, G.; Liska, N.; Evergren, E.; McMahon, H. T.; Kozlov, M. M. *Cell* **2012**, *149*, 124.
(13) Masuda, M.; Takeda, S.; Sone, M.; Ohki, T.; Mori, H.; Kamioka, Y.; Mochizuki, N. *EMBO J.* **2006**, *25*, 2889.
(14) Frost, A.; Unger, V. M.; De Camilli, P. *Cell* **2009**, *137*, 191.
(15) Baumgart, T.; Capraro, B. R.; Zhu, C.; Das, S. L. *Annu. Rev. Phys. Chem.* 2011, *62*, 483.
(16) Schmidt, A.; Wolde, M.; Thiele, C.; Fest, W.; Kratzin, H.; Podtelejnikov, A. V.; Witke, W.; Huttner, W. B.; Soling, H. D. *Nature* **1999**, *401*, 133.
(17) Ringstad, N.; Nemoto, Y.; DeCamilli, P. *Proc. Natl. Acad. Sci. U. S. A.* **1997**, *94*, 8569.
(18) Milosevic, I.; Giovedi, S.; Lou, X. L.; Raimondi, A.; Collesi, C.; Shen, H. Y.; Paradise, S.; O'Toole, E.; Ferguson, S.; Cremona, O.; De Camilli, P. *Neuron* **2011**, *72*, 587.
(19) Vázquez, F. X.; Unger, V. M.; Voth, G. A. *Biophys. J.* **2013**, *104*, 396.
(20) Wang, Q.; Kaan, H. Y. K.; Hooda, R. N.; Goh, S. L.; Sondermann, H. *Structure* **2008**, *16*, 1574.
(21) Meinecke, M.; Boucrot, E.; Camdere, G.; Hon, W. C.; Mittal, R.; McMahon, H. T. *J. Biol. Chem.* **2013**, *288*, 6651.
(22) Ozeki, S.; Kato, T.; Holtzer, M. E.; Holtzer, A. *Biopolymers* **1991**, *31*, 957.
(23) Merickel, S. K.; Sanders, E. R.; Vázquez-Ibar, J. L.; Johnson, R. C. *Biochemistry* **2002**, *41*, 5788.
(24) Moore, J. M. R.; Patapoff, T. W.; Cromwell, M. E. M. *Biochemistry* **1999**, *38*, 13960.
(25) Kitano, H.; Maeda, Y.; Okubo, T. *Biophys. Chem.* **1989**, *33*, 47.
(26) Maeda, H.; Engel, J.; Schramm, H. J. *Eur. J. Biochem.* **1976**, *69*, 133.
(27) Bosshard, H. R.; Durr, E.; Hitz, T.; Jelesarov, I. *Biochemistry* **2001**, *40*, 3544.
(28) Parr, G. R.; Hammes, G. G. *Biochemistry* **1976**, *15*, 857.
(29) Schreiber, G.; Haran, G.; Zhou, H. X. *Chem. Rev.* **2009**, *109*, 839.
(30) Capraro, B. R.; Shi, Z.; Wu, T.; Chen, Z.; Dunn, J. M.; Rhoades, E.; Baumgart, T. *J. Biol. Chem.* **2013**, *288*, 12533.
(31) Nooren, I. M. A.; Thornton, J. M. *J. Mol. Biol.* **2003**, *325*, 991.
(32) Dey, S.; Pal, A.; Chakrabarti, P.; Janin, J. *J. Mol. Biol.* **2010**, *398*, 146.
(33) Wendt, H.; Berger, C.; Baici, A.; Thomas, R. M.; Bosshard, H. R. *Biochemistry* **1995**, *34*, 4097.
(34) Jonsson, T.; Waldburger, C. D.; Sauer, R. T. *Biochemistry* **1996**, *35*, 4795.
(35) Merzlyakov, M.; Chen, L.; Hristova, K. *J. Membr. Biol.* **2007**, *215*, 93.
(36) Jia, H. F.; Satumba, W. J.; Bidwell, G. L.; Mossing, M. C. *J. Mol. Biol.* **2005**, *350*, 919.
(37) Schreiber, G. *Curr. Opin. Struct. Biol.* **2002**, *12*, 41.
(38) Myers, J. K.; Pace, C. N.; Scholtz, J. M. *Protein Sci.* **1995**, *4*, 2138.
(39) Zhou, H. X. Q. *Rev. Biophys.* **2010**, *43*, 219.
(40) Janin, J. *Biochimie* **1995**, *77*, 497.
(41) Ross, P. D.; Subramanian, S. *Biochemistry* **1981**, *20*, 3096.
(42) Krissinel, E.; Henrick, K. *J. Mol. Biol.* **2007**, *372*, 774.
(43) Neet, K. E.; Timm, D. E. *Protein Sci.* **1994**, *3*, 2167.
(44) Darke, P. L.; Jordan, S. P.; Hall, D. L.; Zugay, J. A.; Shafer, J. A.; Kuo, L. C. *Biochemistry* **1994**, *33*, 98.
(45) Grant, S. K.; Deckman, I. C.; Culp, J. S.; Minnich, M. D.; Brooks, I. S.; Hensley, P.; Debouck, C.; Meek, T. D. *Biochemistry* **1992**, *31*, 9491.
(46) Wang, J. H.; Robinson, C. V.; Edelman, I. S. *J. Am. Chem. Soc.* **1953**, *75*, 466.
(47) Pruppach, H. *J. Chem. Phys.* **1972**, *56*, 101.
(48) Qin, S.; Pang, X. D.; Zhou, H. X. *Structure* **2011**, *19*, 1744.
(49) Lyskov, S.; Chou, F.-C.; Conchúir, S. Ó.; Der, B. S.; Drew, K.; Kuroda, D.; Xu, J.; Weitzner, B. D.; Renfrew, P. D.; Sripakdeevong, P.; Borgo, B.; Havranek, J. J.; Kuhlman, B.; Kortemme, T.; Bonneau, R.; Gray, J. J.; Das, R. *PLoS ONE* **2013**, *8*, e63906.
(50) Lyskov, S.; Gray, J. J. *Nucleic Acids Res.* **2008**, *36*, W233.
(51) Ferraro, E.; Peluso, D.; Via, A.; Ausiello, G.; Helmer-Citterich, M. *Nucleic Acids Res.* **2007**, *35*, W451.
(52) Mim, C.; Cui, H. S.; Gawronski-Salerno, J. A.; Frost, A.; Lyman, E.; Voth, G. A.; Unger, V. M. *Cell* **2012**, *149*, 137.